SUPER SUB-NYQUIST SINGLE-PIXEL THZ IMAGING USING HADAMARD BASIS**

J. Guo [1,2], Q. Ch. Liu [1,3], H. Deng [1,3], G. L. Li [1,3], L. P. Shang [1,3]*

[1] School of Information Engineering, Southwest University of Science and Technology, Mianyang, China; e-mail: 121992278@qq.com
[2] TianFu college of Southwestern University of Finance and Economics, Mianyang, China
[3] Tianfu Institute of Research and Innovation, Southwest University of Science and Technology, Chengdu, China

We present a super sub-Nyquist Hadamard single-pixel THz imaging system in which the THz waves are modulated by a digital micromirror device and a laser driver. Spatial coding of the THz radiation is performed using the cake-cutting (CC)-order Hadamard basis. THz images are reconstructed from a series of coding sequences of the measurement intensity. We prove that with the use of super sub-Nyquist sampling, single-pixel THz imaging with 87% fidelity and a signal-to-noise ratio of more than 23 dB can be achieved using 10% of the CC-order Hadamard basis patterns. The total variation regularization algorithm is shown to have higher robustness to noise than the Hadamard transform and thus offers a good technical solution for single-pixel THz imaging.

Keywords: *terahertz single pixel imaging, compressed sensing, Hadamard basis, Hadamard transform, TVAL3 algorithm.*

МЕТОД СОЗДАНИЯ СУБНАЙКВИСТОВСКИХ ОДНОПИКСЕЛЬНЫХ ИЗОБРАЖЕНИЙ С ИСПОЛЬЗОВАНИЕМ БАЗИСА АДАМАРА

J. Guo [1,2], Q. Ch. Liu [1,3], H. Deng [1,3], G. L. Li [1,3], L. P. Shang [1,3]*

УДК 535.317.1

[1] Школа информационной инженерии Юго-Западного университета науки и технологий, Мяньян, Китай; e-mail: 121992278@qq.com
[2] Колледж ТяньФу Юго-Западного университета финансов и экономики, Мяньян, Китай
[3] Институт исследований и инноваций Тяньфу Юго-Западного университета науки и технологий, Чэнду, Китай

(Поступила 23 ноября 2022)

Предложена однопиксельная терагерцовая (ТГц) система визуализации суперсуб-Найквиста-Адамара, в которой ТГц-волны модулируются цифровым микрозеркальным устройством и лазерным драйвером. Пространственное кодирование ТГц-излучения осуществляется с помощью базиса Адамара порядка СС. ТГц-изображения реконструируются из серии последовательностей кодирования измерений интенсивности. Доказано, что при дискретизации суперсуб-Найквиста однопиксельное ТГц-изображение с точностью 87% и отношением сигнал/шум >23 дБ может быть получено с использованием 10% базисных шаблонов Адамара порядка СС. Алгоритм регуляризации полной вариации обладает более высокой устойчивостью к шуму, чем преобразование Адамара, и является хорошим техническим вариантом для однопиксельного ТГц-изображения.

Ключевые слова: *однопиксельное изображение в терагерцовом диапазоне, сжатое зондирование, базис Адамара, преобразование Адамара, TVAL3-алгоритм.*

** Full text is published in JAS V. 90, No. 5 (http://springer.com/journal/10812) and in electronic version of ZhPS V. 90, No. 5 (http://www.elibrary.ru/title_about.asp?id=7318; sales@elibrary.ru).

Introduction. Terahertz (THz) imaging has been receiving increasing attention in the last years [1, 2]. THz radiation forms the part of the electromagnetic spectrum that lies between the infrared and microwave bands. Therefore, THz radiation combines the electronic and photonic features of both microwaves and infrared light. This emerging imaging technique has found an extensive range of applications recently. THz radiation is transient and penetrating, carries low energy, and can be used to perform fingerprint imaging. The THz spectral region also contains large amounts of physical and chemical structure information. THz imaging thus has many potential applications, including nondestructive testing [3, 4], medical diagnosis [5, 6], and art protection [7, 8].

However, few area array detectors with sufficiently high resolution have been available for use in THz imaging. At present, THz imaging involves point-by-point scanning, which is time-consuming and thus restricts the potential for popularization of the technique. The compressed sensing technique [9–11] has been enormously beneficial for use in single-pixel imaging in various wave bands, including the THz [12, 13]. Single-pixel THz imaging primarily uses photoinduced semiconductor optical modulation, where the spatial light modulator is composed of a DMD and a silicon. Specifically, the DMD projects the coded patterns onto the silicon semiconductor to modulate the THz radiation. The correlations between a series of coding sequences of the measurement intensity and the coded patterns are used, and the images are then reconstructed using the TVAL3 algorithm.

Busch [14] proved that spatial modulation of THz waves could be achieved via photoinduced behavior in semiconductors and analyzed the possibility of optically-controlled THz imaging. Shams et al. [15] used a combination of DMD-projected Hadamard basis patterns and a compressive sensing algorithm to achieve single-pixel imaging with a compression ratio of 40%. Augustin et al. [16] designed a germanium disk-based modulator for THz radiation and used a matching pursuit algorithm to perform image reconstruction; a good reconstruction performance with a compression ratio of 30% was reported. Stantchev et al. [17, 18] demonstrated subwavelength near-field THz imaging and proposed an adaptive sampling technique, which allowed the target images to be obtained despite a low compression ratio of 35%. Lu et al. [19] built a reflective single-pixel THz imaging system in which a compressive sensing algorithm was integrated with an inverse Fresnel diffraction algorithm. This method provided a satisfactory rendering for the reconstruction of metal letter images at a compression ratio of 25%. Zanotto et al. [20] introduced modulated light beams into a conventional THz time-domain spectroscopy system to perform single-pixel far-field THz imaging; multidimensional imaging was performed at sampling rates of less than 50%.

The number of Hadamard basis patterns that are projected during single-pixel THz imaging has a direct bearing on the imaging speed, with the number of Hadamard basis patterns required increasing dramatically when high-resolution THz imaging is performed. At present, the compression ratio required in single-pixel THz imaging remains high. Appropriate selection of the Hadamard basis patterns has thus been studied extensively [21, 22]. Sun et al. [23] proposed Russian doll (RD) ordering, while Yu [24] described cake-cutting (CC) ordering. They observed that fewer connected domains in each pattern would lead to more significant measurements being obtained. Yu et al. [25] ordered their Hadamard basis patterns using the total variation (TV) of each reshaped mask for general scenes and subsequently obtained well-reconstructed images.

The studies above are very helpful when searching for the most significant patterns that can be used for single-pixel THz imaging. In our research, we introduce a modulated optical path into an existing THz time-domain spectroscopy system and construct a single-pixel THz imaging system. A DMD is used to project CC-order Hadamard basis patterns onto high-resistivity silicon to modulate the THz radiation. Finally, the THz images are reconstructed using a compressed sensing algorithm. We demonstrate image reconstruction at a sampling rate of 10%, which is lower than the rates reported previously in other studies. We believe that imaging at a super-low compression ratio will be highly important for the application and promotion of single-pixel THz imaging.

Single-pixel imaging principle. For the signal $x \in R_{N\times 1}$ there is a measurement matrix $\Phi \in R_{M\times N} (M << N)$ under which the linear measurement is $y \in R_{M\times 1}$ as shown below:

$$y = \Phi x. \tag{1}$$

Equation (1) is regarded as the linear projection of the original signal $\boldsymbol{x}$ under the matrix $\boldsymbol{\Phi}$. This is because the number of dimensions of $\boldsymbol{y}$ is far lower than that of $\boldsymbol{x}$ and the former thus has an infinite number of solutions. For this reason, the original signal can hardly be reconstructed using the former. In contrast, if the original signal $\boldsymbol{x}$ is K-sparse and $\boldsymbol{\Phi}$ satisfies the restricted isometry property, i.e., for any K-sparse signals and a constant $\delta_k \in (0,1)$

$$(1-\delta_k)\|x\|_2^2 \le \|\Phi x\|_2^2 \le (1+\delta_k)\|x\|_2^2, \quad (2)$$

then the signal x can be reconstructed precisely from the measurement of y by solving for the optimal l_0 norm:

$$x = \arg\min \|x_0\| \quad s \cdot t \quad y = \Phi x, \quad (3)$$

where $\|\ldots\|_0$ is the norm of l_0, and the number of measurements M must satisfy $M = O(K\log(N))$. Equation (3) represents a classical NP-hard problem, which is difficult to solve. Candes and Donoho proposed replacing the l_0 norm with the l_1 norm for solving this problem. The solutions to the two problems are equivalent so long as the image is sparsely represented.

The single-pixel detector is used to obtain a series of sequences of measurement intensity, to which the compressive sensing algorithm is applied for reconstructing images. Typical compressive sensing algorithms for this purpose include orthogonal matching pursuit, basis pursuit, and TVAL3. If the Hadamard basis is used, the Hadamard transform is also available for use as a reconstruction algorithm.

Experimental. The optical path structure for the single-pixel THz imaging system is shown in Fig. 1. This system consists of the pump beam, probe beam, and control beam. The pump beam passing through the convex lens is focused on the photoconductive antenna. A bias voltage is imposed on the photoconductive antenna to excite THz waves. The sample and the high-resistivity silicon are placed along the collimating optical path. Indium tin oxide (ITO) is used to reflect the THz radiation that penetrates the sample, and this radiation is ultimately focused and detected using the detection antenna.

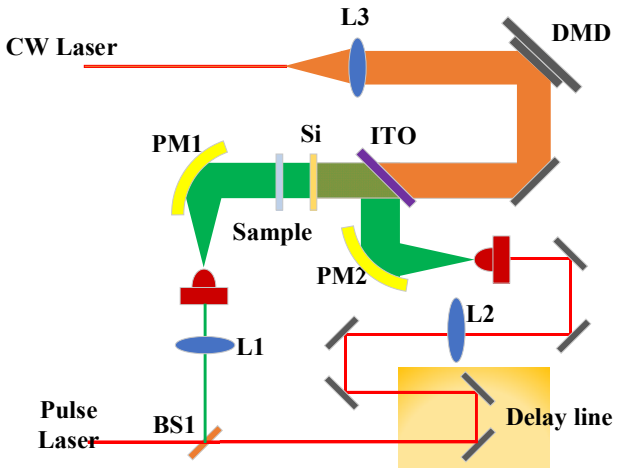

Fig. 1. Optical construction for single-pixel THz imaging.

A delay line is inserted into the probe optical path to adjust the optical path difference and thus achieve superposition of the THz waves and the probe beam. These superposed light beams are then passed through a lock-in amplifier to detect the THz signals. The DMD loads a series of measured masks into the control optical path and these masks are then projected onto the silicon to excite the charge carriers required to modulate the THz beams. This modulation process will affect the measurement intensity. After multiple repeated measurements, the correlation between the measurement intensity data and the measured masks can be used to reconstruct THz images of the sample to be measured. A compressive sensing algorithm is used here to achieve sampling at super-low sampling rates. The pump laser wavelength is 800 nm, the pulse duration is 35 fs, and the oscillation frequency is 80 MHz. The BATOP bPCA-100-05-10-800 photoconductive antenna was used as the THz source and a bias voltage of 100 V was applied. To avoid the complexity that arises from simultaneous setting up of the control and probe optical paths, we used a continuous-wave laser from a BWT diode laser system to irradiate the DMD (V-7000 VIS, Vialux), with highest resolution of 1024×768. The DMD projected Hadamard basis patterns onto the high-resistivity silicon to modulate the THz radiation. The intensity signals of the THz radiation were then detected using the SR380 lock-in amplifier (Stanford Research Systems).

Results and discussion. The hollowed-out metal letters “T”, “H”, and “Z” were used to perform the imaging experiments, where the line width was 2 mm. A sample was placed at a distance of 10 mm from the semiconductor silicon wafer surface. The Hadamard matrix was 32×32. The area projected by the DMD onto the silicon wafer surface was 22 mm×17 mm. Throughout the course of the single-pixel imaging process, the delay line was located at the point where the signal amplitude in the THz time-domain spectrum was at a maximum. CC-order Hadamard basis patterns were used to perform imaging of the metal letters at super-low sampling rates.

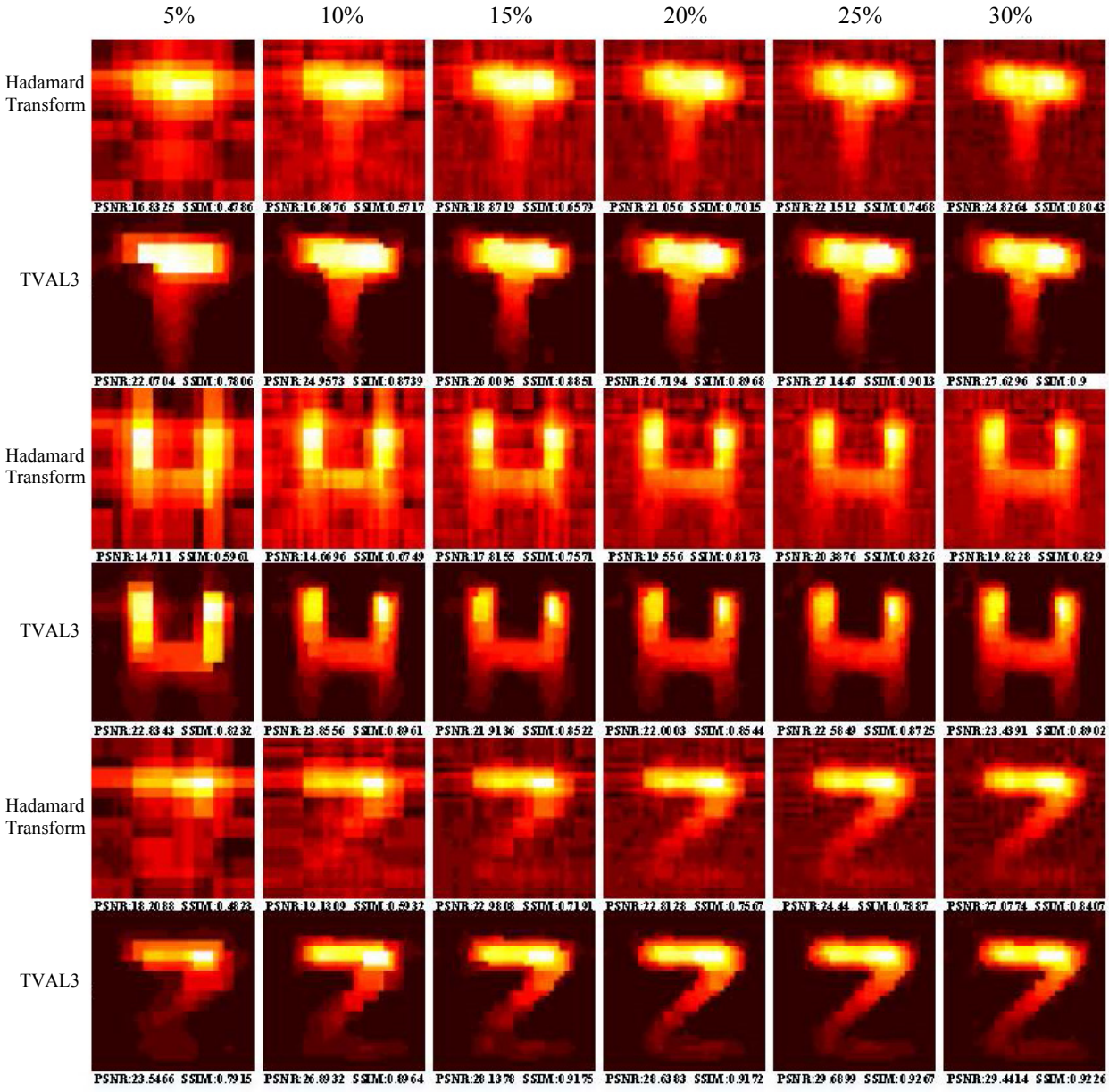

Fig. 2. Reconstructed THz image of the metal letters “T”, “H”, and “Z”.

Two reconstruction algorithms were implemented, comprising the Hadamard transform and TVAL3 algorithms, and a comparison of their performances is shown in Fig. 2. This comparison shows that TVAL3 produced much better reconstructions than the Hadamard transform and also presented a higher anti-noise performance. At the sampling rates of 5% and 10%, use of the Hadamard transform produced heavily blurred images that indicated severe noise; the contours of the samples can barely be discerned. At sampling rates of 15–30%, the Hadamard transform produced a better reconstruction performance as the number of

Hadamard basis patterns used increased, but the noise remained significant. In contrast, the TVAL3 algorithm displayed strong noise robustness. At the sampling rate of 5%, the letters "T" and "H" could be recognized roughly; however, the lower half of the letter "Z" was missing upon reconstruction. This missing detail is probably caused by the nonuniform distribution of the Hadamard basis patterns and the THz intensity spots related to the "Z" letter reconstruction. At the sampling rate of 10%, all three letters could be visualized distinctly. When the sampling rate and the number of Hadamard basis patterns were increased, the reconstruction performance was then improved further. With the CC order, the Hadamard basis patterns with higher coherent areas were selected to perform the modulation. The patterns are ordered in ascending order in terms of the numbers of connected domains in each pattern. The patterns with the highest contributions are projected preferentially to ensure that visually recognizable reconstructions can still be achieved at the super-low sampling rate of 10%.

To quantify the reconstruction performances, we adopted the method presented in [26] and used images that were reconstructed at a sampling rate of 100% using the two reconstruction algorithms (i.e., the Hadamard transform and TVAL3 algorithms) as the ground truth. The structural similarity index (SSIM) and the peak signal-to-noise ratio (PSNR) were calculated as measures of the reconstruction performance. The role of the SSIM is to compare the similarities between the images, where a larger SSIM means greater similarity between the images. The PSNR is used to measure the image quality, where a higher PSNR value means lower distortion of the reconstruction images. The SSIM and PSNR characteristics for each reconstruction algorithm are shown in Fig. 3. The solid lines represent the reconstruction results when using TVAL3 and the dot-dashed lines represent the reconstruction results when using the Hadamard transform. The reconstructed letter "T" was traced in red, the reconstructed "H" was traced in blue, and the reconstructed "Z" was traced in green.

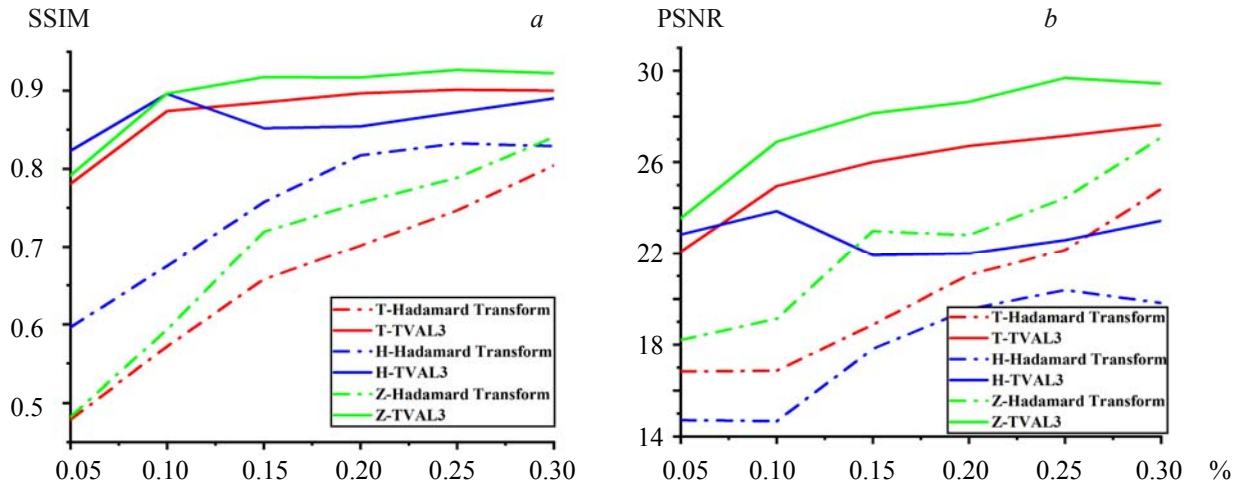

Fig. 3. SSIM (a) and PSNR (b) for single-pixel THz imaging.

Based on consideration of the SSIM, TVAL3 consistently outperformed the Hadamard transform when used at the same sampling rate. When the sampling rate was only 10%, the SSIM values for the three letters all approached 90% using TVAL3, with specific SSIM values of 87%, 89%, and 89%. The high fidelity observed also agreed with the results of the qualitative analysis. When the sampling rate increased to 30%, the SSIM increased slightly. The top-ranking patterns in the CC order made the greatest contributions. The low-ranking patterns made lower contributions to the reconstruction when using TVAL3. Regarding the PSNR, the signal-to-noise ratio was higher when using TVAL3. At the low sampling rate of 10%, the PSNR remained consistently above 23 dB. The PSNR only decreased as the sampling rate increased during reconstruction of the letter "H". This occurred because the newly added Hadamard basis patterns meant that new noise was undesirably introduced into the reconstruction process for this letter.

Conclusions. In the CC order, Hadamard basis patterns with larger coherent areas are selected for modulation of THz radiation [27]. The top-ranking patterns make the greatest contributions by preserving the majority of the information. In this study, we constructed a single-pixel imaging system with photo-excited THz waves. The CC-order Hadamard basis patterns were used as the measurement matrices in this system.

Then, we conducted imaging experiments to compare use of the Hadamard transform and TVAL3 for the reconstruction process. Although the Hadamard transform can at least theoretically achieve perfect reconstruction under the 100% sampling rate condition, we did not observe excellent reconstruction performances during our experiments. Instead, TVAL3 displayed stronger noise robustness. We were surprised to find that TVAL3 with the CC-order Hadamard basis patterns provided better results for high-fidelity single-pixel THz imaging at a sampling rate of 10%. The ability to perform THz imaging at super-low sampling rates will be highly important in enabling extensive application of this emerging imaging technique.

Acknowledgements. This work was supported by the National Natural Science Foundation of China (No. 11872058); the Doctor Foundation of Southwest University of Science and Technology (21ZX7143); the Natural Science Foundation of Southwest University of Science and Technology (No. 21ZX7127); and the Sichuan Science and Technology Program of China (No. 2019ZDZX0013).

REFERENCES

1. P. Hillger, J. Grzyb, R. Jain, U. R. Pfeiffer, *IEEE THz Sci. Tech.*, **9**, No. 1, 1–19 (2019).
2. Q. Wang, L. Xie, Y. Ying, *Appl. Spectrosc. Rev.*, **57**, No. 3, 249–264 (2021).
3. C. Jansen, S. Wietzke, O. Peters, M. Scheller, N. Vieweg, M. Salhi, N. Krumbholz, C. Joerdens, T. Hochrein, M. Koch, *Appl. Optics*, **49**, No. 19, E48–E57 (2010).
4. S. C. Zhong, *Front Mech. Eng.*, **14**, No. 3, 273–281 (2019).
5. M. Danciu, T. Alexa-Stratulat, C. Stefanescu, G. Dodi, B. I. Tamba, C. T. Mihai, G. D. Stanciu, A. Luca, I. A. Spiridon, L. B. Ungureanu, V. Ianole, I. Ciortescu, C. Mihai, G. Stefanescu, I. Chirila, R. Ciobanu, V. L. Drug, *Mater*., **12**, No. 9, 16 (2019).
6. X. Yang, X. Zhao, K. Yang, Y. P. Liu, Y. Liu, W. L. Fu, Y. Luo, *Trends Biotechnol.*, **34**, No. 10, 810–824 (2016).
7. J. Dong, A. Locquet, M. Melis, D. S. Citrin, *Sci. Rep.*, **7** (2017).
8. E. Abraham, A. Younus, J. C. Delagnes, P. Mounaix, *Appl. Phys. A*, **100**, No. 3, 585–590 (2010).
9. E. J. Candes, J. Romberg, T. Tao, *IEEE Inform. Theory*, **52**, No. 2, 489–509 (2006).
10. E. J. Candes, T. Tao, *IEEE Inform. Theory*, **52**, No. 12, 5406–5425 (2006).
11. D. L. Donoho, *IEEE Inform. Theory*, **52**, No. 4, 1289–1306 (2006).
12. H. Shapiro, J. I. Jeffrey, *Phys. Rev. A*, **78**, No. 6, 061802 (2008).
13. N. Gopalsami, S. Liao, T. W. Elmer, E. R. Koehl, A. Heifetz, A. C. Raptis, L. Spinoulas, A. K. Katsaggelos, *Opt Eng*., **51**, No. 9, 091614(1–5) (2012).
14. S. Busch, B. Scherger, M. Scheller, M. Koch, *Opt. Lett.*, **37**, No. 8, 1391–1393 (2012).
15. M. I. B. Shams, L. Liu, S. Rahman, L. J. Cheng, P. Fay, Z. Jiang, J. Qayyum, H. G. Xing, *Electron Lett.*, **50**, No. 11, 801–803 (2014).
16. S. Augustin, J. Hieronymus, P. Jung, H. W. Hübers, *J. Infrared Millim.*, **36**, No. 5, 496–512 (2015).
17. R. I. Stantchev, B. Sun, S. M. Hornett, P. A. Hobson, G. M. Gibson, M. J. Padgett, E. Hendry, *Sci. Adv.*, **2**, No. 6 (2016).
18. R. I. Stantchev, D. B. Phillips, P. Hobson, S. M. Hornett, M. J. Padgett, E. Hendry, *Optica*, **4**, No. 8, 989–996 (2017).
19. Y. Lu, X.-K. Wang, W.-F. Sun, S.-F. Feng, J.-S. Ye, P. Han, Y. Zhang, *IEEE THz Sci. Tech.*, **10**, No. 5, 495–501 (2020).
20. L. Zanotto, R. Piccoli, J. Dong, D. Caraffini, R. Morandotti, L. Razzari, *Opt. Express*, **28**, No. 3, 3795–3802 (2020).
21. T. A. Lu, Z. Qiu, Z. Zhang, J. Zhong, *Opt. Laser Eng.*, **134** (2020).
22. P. G. Vaz, D. Amaral, L. F. Requicha Ferreira, M. Morgado, J. Cardoso, *Opt. Express*, **28**, No. 8, 11666–11681 (2020).
23. M. J. Sun, L. T. Meng, M. P. Edgar, M. J. Padgett, N. Radwell, *Sci. Rep.*, **7**, No. 1, 3464 (2017).
24. W. K. Yu, *Sensors* (Basel), **19**, No. 19, 4122 (2019).
25. X. Yu, R. I. Stantchev, F. Yang, E. Pickwell-MacPherson, *Sci. Rep.*, **10**, No. 1, 9338 (2020).
26. L. Lopez-Garcia, W. Cruz-Santos, A. Garcia-Arellano, P. Filio-Aguilar, J. A. Cisneros-Martinez, R. Ramos-Garcia, *Opt. Express*, **30**, No. 8, 13714–13732 (2022).
27. M.-F. Li, L. Yan, R. Yang, Y.-X. Liu, *Acta Phys. Sin.*, **68**, No. 6, 064202 (2019).